

# APPLICATION OF A STATE-SPACE WAKE MODEL TO TILTROTOR WING UNSTEADY AERODYNAMICS

Martin Stettner                      Daniel P. Schrage  
Graduate Research Assistant      Professor  
Georgia Institute of Technology  
Atlanta, Georgia 30332

David A. Peters  
Professor  
Washington University  
St. Louis, Missouri 63130

## Abstract

The Peters/He Finite State Wake Model is described in its application to fixed wing aerolasticity. Expressions for coupling this model with a wing, aerodynamically represented by a flat plate with a trailing edge flap, are developed, and fidelity issues are discussed. An application is presented where the wing/wake system is coupled to a proprotor model. The effects of unsteady wing aerodynamics on damping of this system are investigated. It is found that wake effects are small as a result of generally low damping levels in the system due to wing aerodynamic damping.

## Notation

AR	aspect ratio
C	linear differential operator
$C_m^n, D_m^n$	coefficients, eq. (6) and (7)
D	drag/unit length
$D_i, D_i^*$	coefficients, eq. (34)
L	lift/unit length; linear diff. operator
M	moment/unit length; max. order of radial polynomials
[M]	wake mass matrix
[N]	wake damping matrix
P	pressure discontinuity
$P_m^n, Q_m^n$	associated Legendre Polynomials of first and second kind
R	disk radius
S	wing semi span
U	freestream velocity
V	disturbance velocity
$a_m^n, b_m^n$	wake states
b	wing semi chord
i	coordinate index; index

n, j	polynomial number
m, r	harmonics number
f	frequency [Hz]
k	reduced frequency
q	perturbation velocity
r	radial coordinate
t	time
u, w	chord/beamwise wing deflection
x, y, z	cartesian coordinates
$\Delta$	relative deviation, (value-ref.)/ref.
$\Lambda$	wing sweep angle
$\Phi$	pert. pressure; acceleration potential
$\alpha$	airfoil pitch angle
$\alpha_0$	airfoil pitch angle, steady state
$\delta$	flap deflection angle
$\lambda$	wake induced velocity
$\overline{\lambda}_{i,j}$	integrals, eq. (21)
v, $\mu$ , $\psi$	ellipsoidal coordinates
$\Psi$	azimuthal coordinate
$\rho$	density
$\theta$	chordwise coordinate
$\phi$	pressure discontinuity at the disk
$\tau_m^n$	wake generalized forcing function
$\omega$	normalwash on airfoil/flap
$\xi$	coordinate in freestream direction
$\chi$	wake skew angle

### Subscripts:

.i	derivative wrt. coordinate i
d	flap hinge location
h	horizontal
v	vertical
n,j	polynomial number
. $\xi$	derivative in freestream direction
$\tau$	circulatory

### Superscripts:

A	acceleration part
V	momentum flux part
c	cosine partition
le	leading edge
m, r	harmonics number
te	trailing edge

---

Presented at the American Helicopter Society Aeromechanics Specialists Conference, San Francisco, California, January 19-21, 1994. Copyright © 1994 by the American Helicopter Society Inc. All rights reserved.

Symbols:

$( )^*$	derivative wrt. nondimensional time
$( \bar{ } )$	normalized value; for ... by ...:
	length R
	speed U
	time R/U
	frequency U/R
	lift/unit length $\rho U^2 R$
	pressure $\rho U^2 R^2$
	moment/unit l. $\rho U^2 R^2$
[ ]	matrix
{ }	column vector

## Introduction

The tiltrotor aircraft currently receives a lot of attention as a possible solution to airport congestion problems. Recent preliminary design trend and optimization studies like reference [1] show that this configuration has the potential of being economically competitive with turboprop aircraft. These studies usually include only an approximate representation of the effect of proprotor whirl flutter, a coupled rotor-wing instability and major design driver for this configuration. The current state-of-the-art computer program for V/STOL aircraft, VASCOMP [2], for example, accounts for this phenomenon by placing the first three wing natural frequencies at particular fractions of rotor rpm. This approach does not account for any coupling between these modes, rotor dynamic characteristics, or flutter alleviation by active controls. Previous research in the latter areas, on the other hand, did not include integration with aircraft sizing/mission performance analysis and optimization ([3], [4]). A current research effort at Georgia Tech's School of Aerospace Engineering therefore focuses on integrating aircraft sizing, wing structural design, wing aerodynamics, rotor aeroelasticity and control system design into a Multidisciplinary Optimization (MDO) framework [5].

Two areas are particularly under investigation. The first is an improved structural model of the wing which accounts for dynamic tailoring through the use of composite materials, without requiring excessive computational effort. The Equivalent Laminated Plate Solution ELAPS [6] proved to be sufficiently accurate for this task, while being computationally more efficient than Finite-Element analyses. The second focus is on inclusion of unsteady wing/flap aerodynamics. Previous studies included only a quasi-steady representation, although the natural frequency of the flutter mode found by van Aken [7] for an XV-15-type wing-rotor configuration translate into reduced frequencies around 0.16. A closer investigation of the effect of unsteady aerodynamics

on the proprotor whirl phenomenon seems therefore necessary.

Most fixed-wing flutter analyses employ k-type aerodynamics like the Doublet-Lattice or Vortex-Lattice Method, Kernel Function approaches, or Strip Theory with Theodorsen Function correction. Since k-type aerodynamics are formulated for simple harmonic motion, they are not directly applicable to modal analysis of an aerodynamically damped system and subsequent flutter suppression controller design. In the case of the first task, iteration on the imaginary part of the eigenvalues is required (p-k-Method). For the second task, the aerodynamic influence coefficients for simple harmonic motion (purely imaginary eigenvalues/k-type) need to be expanded into the complex plane using Padé-Approximation [8] or Minimum-State rational function approximation techniques. Both approaches require calculation of the unsteady aerodynamic influence coefficient matrix for several reduced frequencies. In summary: Utilization of k-type aerodynamics turns conversion of the aeroelastic system to state-space form into an inconvenient process. For aeroservoelastic applications, an unsteady aerodynamics model formulated in state-space form is clearly preferable.

## Peters/He Wake Model

Such a model was developed by Peters and He for rotary wing applications [9]. It is currently being implemented in the aeroelastic stability analysis of rotary wing computer codes like CAMRAD and 2GCHAS for its simplicity and accuracy. Nibbelink and Peters [10] showed also its applicability to fixed wing aeroelasticity. For a lifting-line lift model and a pressure distribution assumed constant along the chord, rectangular, large aspect ratio wing planform, and simple harmonic motion the results correlated acceptably with Theodorsen Theory. The following paragraphs are meant to provide an overview of the general philosophy of the approach and a review of references [9] to [11], rather than a detailed description.

For incompressible flow with small perturbations, the continuity and the momentum equation can be written in index notation:

$$q_{i,i} = 0 \quad (1)$$

$$q_i^* - V_\infty q_{i,\xi} = -\Phi_{,i} \quad (2)$$

where  $V_\infty$  is the nondimensional freestream velocity (divided by rotor tip speed in rotary wing applications; for fixed wing, this term is unity),  $q_i$  are the perturbation velocity components and  $q_i^*$ ,  $q_{i,\xi}$ ,

and  $q_{i,j}$  their derivatives with respect to nondimensional time, along freestream direction, and along coordinate direction, respectively. The form of equation (1) suggests separation of the perturbation pressure  $\Phi$  into a part resulting from acceleration  $\Phi^A$  and a part stemming from the momentum flux  $\Phi^V$ , so that

$$\Phi = \Phi^A + \Phi^V \quad (3)$$

where

$$\Phi^V_{,i} = V_\infty q_{i,\xi} \quad (4)$$

and

$$\Phi^A_{,i} = -q_i^* \quad (5)$$

By differentiating (2) with respect to  $i$  and applying the continuity equation (1) it can be shown that both parts of the perturbation pressure must satisfy Laplace's equation and therefore resemble acceleration potentials. One solution for Laplace's equation is known as Prandtl's acceleration potential function for circular wings in the ellipsoidal coordinates  $v$ ,  $\eta$ , and  $\psi$

$$\Phi(v, \eta, \psi, \bar{t}) = \sum_{m,n} P_n^m(v) Q_n^m(i\eta) [C_n^m(\bar{t}) \cos(m\psi) + D_n^m(\bar{t}) \sin(m\psi)] \quad (6)$$

using the Legendre Polynomials of the first and second kind,  $P_n^m$  and  $Q_n^m$ , and coefficients  $C_n^m$  and  $D_n^m$ . On the rotor disk ( $\eta = 0$ ,  $v = \sqrt{1 - \bar{r}^2}$ ) this function models a pressure discontinuity with a pressure difference,  $\phi$ , between upper and lower side of the circular lifting surface\*

$$\phi(\bar{r}, \psi, \bar{t}) = -2 \sum_{m,n} P_n^m(v) Q_n^m(i0) [C_n^m(\bar{t}) \cos(m\psi) + D_n^m(\bar{t}) \sin(m\psi)] \quad (7)$$

If the perturbation velocity normal to the rotor disk,  $q_z$ , is denoted by  $\lambda$ , Equations (4) and (5) can be rewritten in the form

$$\lambda(\bar{r}, \psi, \bar{t}) = \frac{1}{V_\infty} \int_{-\infty}^0 \left( \frac{\partial \Phi^V}{\partial z} \right) d\xi \equiv L[\Phi^V] \quad (8)$$

$$\lambda^* = \left( \frac{\partial \Phi^A}{\partial \xi} \right)_{\eta=0} \equiv C[\Phi^A] \quad (9)$$

$L$  and  $C$  are linear operators on  $\Phi^A$  and  $\Phi^V$ . Provided that these two operators are invertible, a first order differential equation in  $\lambda$  can be written:

$$C^{-1}[\lambda^*] + L^{-1}[\lambda] = \Phi^A + \Phi^V = \phi \quad (10)$$

The inversion is possible if the induced velocity is expanded in terms of harmonics azimuthally and arbitrary functions radially, e.g.

$$\lambda(\bar{r}, \psi, \bar{t}) = \sum_{m,n} \bar{P}_n^m(v) / v [a_n^m(\bar{t}) \cos(m\psi) + b_n^m(\bar{t}) \sin(m\psi)] \quad (11)$$

introducing the inflow states  $a_n^m$  and  $b_n^m$  as coefficients of the azimuthal harmonic,  $m$ , and the radial expansion function,  $n$ . The bar over the Legendre Polynomial symbolizes normalization to a unit integral over the interval  $v = [0,1]$ . Substituting  $\lambda$  as in Equation (11) into the differential equation (10), premultiplying by  $\bar{P}_n^m$  and  $\cos(m\psi)$  and integrating over the rotor disk yields a set of first order ordinary differential equations in  $a_j^m$ :

$$[M^c] \{ \{ a_j^m \} \}^* + [N^c] \{ \{ a_j^m \} \} = \frac{1}{2} \{ \{ \tau_n^{mc} \} \} \quad (12)$$

and an equivalent equation for the  $b_j^m$ , multiplied by  $\sin(m\psi)$  (replace superscript  $c$  by  $s$ ). Since the inflow dynamics (i.e. the rotor wake, or the perturbation velocities induced by a wing) are expressed in state-space form, it is immediately obvious that the model is equally applicable to harmonic and non-harmonic excitation.

The wake 'mass' matrix  $[M]$  and 'damping' matrix  $[N]$  are known functions of the wake skew angle,  $\chi$ .  $[N]$  is in fact the inverse of another matrix originating from the operator  $L$ . Wang [11] developed closed form solutions for this inverse in edgewise flow ( $\chi = 90^\circ$ ) for an infinite number of wake states. For a yet not fully understood reason these solutions are also accurate for two special kinds of truncated systems: (a) cos-partition, maximum order of azimuthal harmonics odd; and (b) sin-partition; maximum order

\* in the following called 'rotor disk': it is, in fact, a circular surface in which pressure discontinuities may occur. For fixed wing applications, it is a disk circumscribing and encompassing the wing, for rotary wing cases it is simply the rotor disk.

of azimuthal harmonics even [11]. Since in fixed wing aeroelastic analyses symmetric and antisymmetric modes are usually treated separately (i.e. either the cos- or the sin-partition is used), these conditions do not create an empty set of options for the analyst striving to reduce computational effort by bypassing a numerical inversion. The following discussion concentrates on the cos-partition, i.e. modeling of symmetric problems.

The right hand side of equation (12) represents the wake system excitation through an imposed pressure discontinuity,  $\bar{P}$  (here nondimensional), across the rotor disk.

$$\tau_n^{mc} = \frac{1}{\pi} \int_0^{2\pi} \int_0^1 \bar{P}(\bar{r}, \psi, \bar{t}) \bar{P}_n^m(v)/v d\bar{r} \cos(m\psi) d\psi \quad (13)$$

or, expressed in cartesian coordinates (refer to Fig. 1):

$$\tau_n^{mc} = \frac{1}{\pi} \int_{-\bar{S}}^{\bar{S}} \int_{\bar{x}_{le}}^{\bar{x}_{te}} \bar{P}(\bar{x}, \bar{y}, \bar{t}) \bar{P}_n^m(v)/v \cos(m\psi) d\bar{x} d\bar{y} \quad (14)$$

In the special case  $m = 0$  (uniform inflow), the expression is divided by 2.

### Wake System Forcing Functions

Obviously, the actual form of these forcing functions depends on the way the pressure discontinuity (or lift) is distributed over the disk, or on the distribution of pressure over the lifting surfaces. One of the key features of the Peters/He wake model is the separation of wake dynamics and lifting surface aerodynamics, as displayed in equation (13). The inflow model is therefore concerned with the effects of shed vorticity only. As a result, (a) only circulatory lift enters the system through  $\bar{P}$ , and (b) the effects of bound circulation are filtered out through choice of a chordwise vorticity distribution which does not induce any velocity on the airfoil (where the wake induced velocity is sought - [9], [10], [12]). Reference [9] lists a number of these candidate distributions. One of them is the solution for the flat plate airfoil,

$$\bar{P}(\bar{x}, \bar{y}, \bar{t}) = \frac{\bar{L}_\tau(\bar{y}, \bar{t})}{\pi \bar{b}(\bar{y})} \tan \frac{\theta}{2} \quad (15)$$

where  $\bar{L}_\tau(\bar{y}, \bar{t})$  is the nondimensional circulatory lift as a function of the spanwise coordinate, and the nondimensional chordwise coordinate,  $\theta$ , for a wing planform as depicted in Fig. 1 is

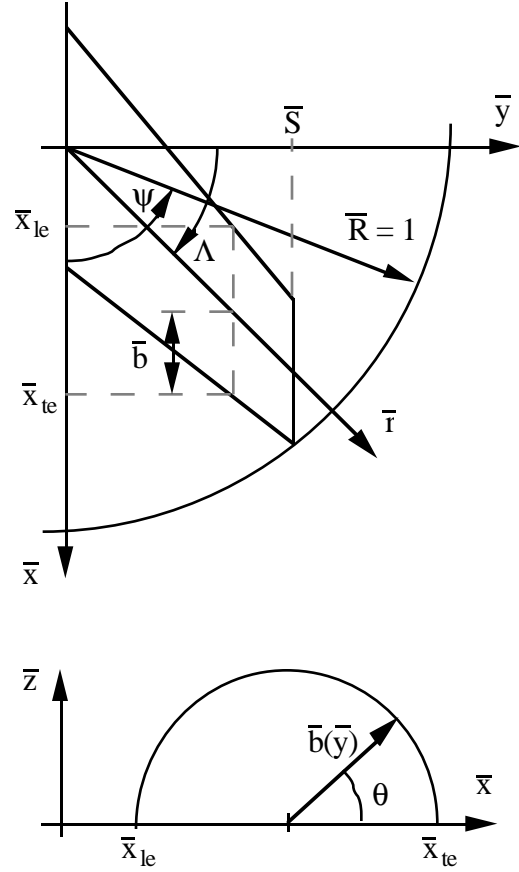


Fig. 1: Coordinate Systems

$$\cos \Theta = (x - y \tan \Lambda) / b(y) \quad (16)$$

Another possible solution, however, has been previously chosen [12]. This particular distribution was selected here since it allows a simplification when expanding the integral (14):

$$\bar{P}(\bar{x}, \bar{y}, \bar{t}) = \frac{\bar{L}_\tau(\bar{y}, \bar{t})}{\pi \bar{b}(\bar{y}) \sin \theta} \quad (17)$$

First,  $\bar{L}_\tau(\bar{y}, \bar{t})$  is expanded. The normalwash at a lifting surface chord due to airfoil shape and motion, denoted by  $\omega(x)$ , and the induced velocity  $\lambda(x)$  can be expanded in a Fourier Series:

$$\omega(x) = \sum_{n=0}^{\infty} \omega_n \cos(n\Theta); \lambda(x) = \sum_{n=0}^{\infty} \lambda_n \cos(n\Theta) \quad (18)$$

The nondimensional circulatory lift can now be expressed in the following form:

$$\begin{aligned} \bar{L}_\tau(\bar{y}, \bar{t}) = 2\pi\bar{b}(\bar{y}) \left( \bar{\omega}_0(\bar{y}, \bar{t}) + \frac{1}{2}\bar{\omega}_1(\bar{y}, \bar{t}) \right) \\ - \bar{\lambda}_0(\bar{y}, \bar{t}) - \frac{1}{2}\bar{\lambda}_1(\bar{y}, \bar{t}) \end{aligned} \quad (19)$$

which allows separation into a wing forcing part (bound circulation) and a wake feedback part. Recalling the definitions for the Fourier Coefficients,

$$\begin{aligned} \bar{\lambda}_0(\bar{y}, \bar{t}) &:= \frac{1}{\pi} \int_0^\pi \bar{\lambda}(\bar{x}, \bar{y}, \bar{t}) d\theta \\ \bar{\lambda}_1(\bar{y}, \bar{t}) &:= \frac{2}{\pi} \int_0^\pi \bar{\lambda}(\bar{x}, \bar{y}, \bar{t}) \cos \theta d\theta \end{aligned} \quad (20)$$

and defining of the integrals

$$\begin{aligned} \bar{\lambda}_{j,0}^{\tau,c}(\bar{y}) &:= \frac{1}{\pi} \int_0^\pi \frac{\bar{P}_j^{\tau,c}(\bar{v})}{\bar{v}} \cos(r \psi) d\theta \\ \bar{\lambda}_{j,1}^{\tau,c}(\bar{y}) &:= \frac{2}{\pi} \int_0^\pi \frac{\bar{P}_j^{\tau,c}(\bar{v})}{\bar{v}} \cos(r \psi) \cos \theta d\theta \end{aligned} \quad (21)$$

the circulatory lift, equation (19) can be rewritten

$$\begin{aligned} \bar{L}_\tau(\bar{y}, \bar{t}) = 2\pi\bar{b}(\bar{y}) \left( \bar{\omega}_0(\bar{y}, \bar{t}) + \frac{1}{2}\bar{\omega}_1(\bar{y}, \bar{t}) \right) \\ - \sum_{r,j} \left( \bar{\lambda}_{j,0}^{\tau,c}(\bar{y}) + \bar{\lambda}_{j,1}^{\tau,c}(\bar{y}) \right) a_j^{\tau,c}(\bar{t}) \end{aligned} \quad (22)$$

Including the pressure distribution (17) in the wake forcing functions (14) and transforming the chordwise coordinate form  $\bar{x}$  to  $\theta$  (using equation (16)) yields

$$\tau_n^{\text{inc}} = \frac{1}{\pi} \int_{-\bar{s}}^{\bar{s}} \bar{L}_\tau(\bar{y}, \bar{t}) \frac{1}{\pi} \int_0^\pi \frac{\bar{P}_n^{\text{inc}}(\bar{v})}{\bar{v}} \cos(m\psi) d\theta d\bar{y} \quad (23)$$

Notice that the inner (chordwise) integral has exactly the same form as  $\bar{\lambda}_{j,0}^{\tau,c}(\bar{y})$  in equation (21), due to the choice of (17) for the chordwise pressure distribution. We finally obtain

$$\begin{aligned} \tau_n^{\text{inc}}(\bar{t}) = 2\pi \int_{-\bar{s}}^{\bar{s}} \bar{b}(\bar{y}) \bar{\lambda}_{n,0}^{\text{inc}}(\bar{y}) \left( \bar{\omega}_0(\bar{y}, \bar{t}) + \frac{1}{2}\bar{\omega}_1(\bar{y}, \bar{t}) \right) d\bar{y} \\ - 2\pi \int_{-\bar{s}}^{\bar{s}} \bar{b}(\bar{y}) \bar{\lambda}_{n,0}^{\text{inc}}(\bar{y}) \sum_{r,j} \left( \bar{\lambda}_{j,0}^{\tau,c}(\bar{y}) + \bar{\lambda}_{j,1}^{\tau,c}(\bar{y}) \right) a_j^{\tau,c}(\bar{t}) d\bar{y} \end{aligned} \quad (24)$$

The question is how the integrals (21) are to be computed. Previous applications in rotary wing aeroelasticity reduced to high aspect ratio rotor blades where a lifting line approximation was justified. Nibbelink [11] also shows for moderate aspect ratio fixed wing cases (AR = 5) acceptable performance. The fact that, in case of a lifting line model, the integration simplifies to evaluation of the expression

$$\bar{\lambda}_{j,0}^{\tau,c}(\bar{y}) := \frac{\bar{P}_j^{\tau,c}(\bar{v})}{\bar{v}} \cos(r(\Lambda - \pi/2)) \quad (25)$$

while  $\bar{\lambda}_{j,1}^{\tau,c}(\bar{y}) = 0$ , certainly makes this option very attractive.

For the next level of fidelity, a large but finite aspect ratio is assumed, and the approximation of small azimuthal deviations from the wing halfchord is made for points on the airfoil:

$$\psi = (\Lambda - \pi/2) + \frac{\bar{b}(\bar{r})}{\bar{r}} \cos \Lambda := (\Lambda - \pi/2) + \tilde{\psi}(\bar{r}) \quad (26)$$

If the chordwise integration is finally approximated by an azimuthal one, the integrals yield Bessel Functions of the first kind as aspect ratio correction factors:

$$\begin{aligned} \bar{\lambda}_{j,0}^{\tau,c}(\bar{y}) &:= \frac{\bar{P}_j^{\tau,c}(\bar{v})}{\bar{v}} J_0(r \tilde{\psi}) \cos(r(\Lambda - \pi/2)) \\ \bar{\lambda}_{j,1}^{\tau,c}(\bar{y}) &:= \frac{\bar{P}_j^{\tau,c}(\bar{v})}{\bar{v}} J_1(r \tilde{\psi}) \cos(r(\Lambda - \pi/2)) \end{aligned} \quad (27)$$

It must be noted that (21) and (25) only converge if the sweep angle  $\Lambda$  approaches zero and the aspect ratio is very large; the same can be shown for the higher order approximation (27). Fig. 2 shows the deviation of  $\bar{\lambda}_{2,0}^{\tau,c}(\bar{y})$  as calculated with equation (27), from the benchmark result from a numerical integration using (21), normalized by this reference value ( $\Delta$ ). Besides the obvious increase in deviation towards the wing root, due to the growing error in the small angle assumption (26), there is also a constant offset - for the first harmonic,  $m = 1$ , the ratio between the results from (21) and (27) is about the cosine of the sweep angle. This appears to relate the deviations directly to the fact that the actual chordwise integration was approximated by an integration along a line perpendicular to the wing's halfchord line. Unfortunately,  $\cos \Lambda$  can only serve as a correction factor for the first harmonic; for higher  $m$ , the influence of the polynomial index  $n$  becomes more pronounced, and the search for a generally valid correction factor for sweep was not successful. In con-

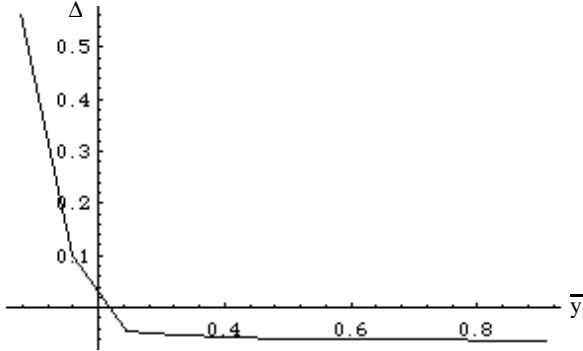


**Fig. 2: Deviation of High Aspect Ratio Approximation from Numerical Integral (aspect ratio of 6, sweep angle 20°)**

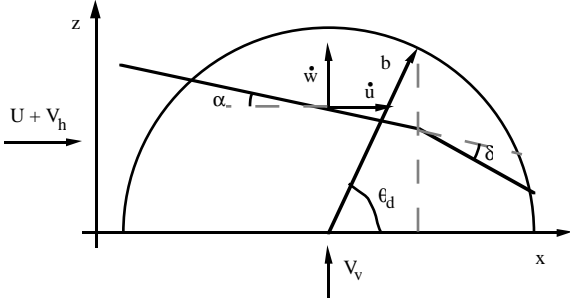


**Fig. 3: Flat Plate with Trailing Edge Flap**

clusion, both the lifting line and high aspect ratio approximation are, strictly speaking, only valid for unswept wings. Since the values of the integrals generally decrease with increasing harmonic and polynomial number, a correction by  $\cos \Lambda$  for  $m = 1$  and restriction to  $\Lambda < 10^\circ$  appear to be reasonable.

### Coupling with Structural System

In order to couple the wake system, equation (11), with a structural system, the generalized forces on structural and wake system must be formulated in terms of the generalized coordinates (or states) of wake and structure. The aerodynamic forcing functions on the structure in  $z$ - and  $x$ - direction, and the pitch up moment, respectively, can for example be found in reference [12]. The drag expression, equation (29), has been linearized.

$$\bar{L}(\bar{y}, \bar{t}) = 2\pi b \bar{(\bar{y})} \left( \bar{\omega}_0(\bar{y}, \bar{t}) + \frac{1}{2} \bar{\omega}_1(\bar{y}, \bar{t}) - \bar{\lambda}_0(\bar{y}, \bar{t}) \right) \quad (28)$$

$$+ \pi b^2 \bar{(\bar{y})} \left( \bar{\omega}_0^*(\bar{y}, \bar{t}) - \frac{1}{2} \bar{\omega}_2^*(\bar{y}, \bar{t}) \right)$$

$$\bar{D}(\bar{y}, \bar{t}) = -2\pi b \bar{(\bar{y})} \alpha_0 \left( 2\bar{\omega}_0(\bar{y}, \bar{t}) + \frac{1}{2} \bar{\omega}_1(\bar{y}, \bar{t}) \right) \quad (29)$$

$$- 2\bar{\lambda}_0(\bar{y}, \bar{t}) - \frac{1}{2} \bar{\lambda}_1(\bar{y}, \bar{t})$$

$$\bar{M}(\bar{y}, \bar{t}) = \pi b^2 \bar{(\bar{y})} \left( \bar{\omega}_0(\bar{y}, \bar{t}) - \frac{1}{2} \bar{\omega}_2(\bar{y}, \bar{t}) - \bar{\lambda}_0(\bar{y}, \bar{t}) \right) \quad (30)$$

$$+ \frac{\pi}{8} b^3 \bar{(\bar{y})} \left( \bar{\omega}_1^*(\bar{y}, \bar{t}) - \bar{\omega}_3^*(\bar{y}, \bar{t}) \right)$$

Note the difference in the lift (28) and the circulatory lift  $\bar{L}_c(\bar{y}, \bar{t})$  (19) used in the wake forcing functions: Equation (28) includes non-circulatory terms, which cancel part of the circulatory terms. Johnson [13] developed expressions for sums of induced flow Fourier coefficients for a flat wake; based on these expressions, one can show that in general

$$\bar{\lambda}_1 + b \left( \bar{\lambda}_0 - \frac{1}{2} \bar{\lambda}_2 \right) = 0$$

$$2(n+1) \bar{\lambda}_{n+1} + b \left( \bar{\lambda}_n - \frac{1}{2} \bar{\lambda}_{n+2} \right) = 0; n > 0 \quad (31)$$

which eliminates  $\bar{\lambda}_1$  from the lift expression, equation (28).

Finally, the normalwash Fourier Coefficients,  $\bar{\omega}_i$ , are expressed in terms of the structural geometry. For the flat plate airfoil with a trailing edge flap as depicted in Fig. 3, the normalwash,  $\bar{\omega}$ , is

$$\theta_d < \theta < \pi:$$

$$\bar{\omega}(\theta, \bar{t}) = \left( 1 + \bar{V}_h(\bar{t}) - \bar{u}^*(\bar{t}) \right) \alpha(\bar{t}) - \bar{w}^*$$

$$+ b \cos \theta \alpha^*(\bar{t}) + \bar{V}_v(\bar{t})$$

$$0 < \theta < \theta_d:$$

$$\bar{\omega}(\theta, \bar{t}) = \left( 1 + \bar{V}_h(\bar{t}) - \bar{u}^*(\bar{t}) \right) \left( \alpha(\bar{t}) + \delta(\bar{t}) \right) - \bar{w}^*$$

$$+ b \cos \theta \left( \alpha^*(\bar{t}) + \delta^*(\bar{t}) \right) - b \cos \theta_d \delta^*(\bar{t}) + \bar{V}_v(\bar{t}) \quad (32)$$

Application of the Fourier transform to (32) and linearization yields the following coefficients:

$$\bar{\omega}_0 = -\bar{w}^* - \alpha_0 \bar{u}^* + \alpha + D_0 \delta + D_0^* b \delta^* + \bar{V}_v + \alpha_0 \bar{V}_h$$

$$\bar{\omega}_1 = b \alpha^* + D_1 \delta + D_1^* b \delta^* \quad (33)$$

$$\bar{\omega}_i = D_i \delta + D_i^* b \delta^*; i > 1$$

$$D_0 = \frac{1}{\pi} \theta_d; D_0^* = -\frac{1}{\pi} (\theta_d \cos \theta_d - \sin \theta_d)$$

$$D_1 = \frac{2}{\pi} \sin \theta_d; D_1^* = \frac{1}{\pi} \left( \theta_d - \frac{1}{2} \sin(2\theta_d) \right)$$

$$D_2 = \frac{1}{\pi} \sin(2\theta_d); D_2^* = \frac{1}{2\pi} \left( \sin(\theta_d) - \frac{1}{3} \sin(3\theta_d) \right) \quad (34)$$

$$D_i = \frac{1}{\pi} \frac{i-1}{i} \sin(i\theta_d); i > 2$$

$$D_i^* = \frac{1}{i\pi} \left( \frac{\sin((i-1)\theta_d)}{i-1} - \frac{\sin((i+1)\theta_d)}{i+1} \right)$$

## Application to a Tiltrotor Wing: Effect of Unsteady Aerodynamics on Proprotor/Wing Eigenvalues

The wake model as described above has been implemented in a FORTRAN program, PWAKE, and incorporated into the Tiltrotor Integrated Design and Analysis Tool, tridat!. The package includes furthermore the wing structural analysis ELAPS [6] and the Proprotor Aeroelastic Stability Analysis PASTA [13]. Fig. 4 provides in overview of the data flow. The package uses UNIX shell scripts for process control and data filtering.

It is instructive to first investigate the behavior of the uncoupled (open-loop) wake system. Table 1 shows the ten eigenvalues of a system with a maximum order of radial polynomials  $M = 7$  (refer to reference [11] regarding the harmonics-polynomial ordering scheme). The eigenvalues are ordered by undamped natural frequency. The first column might require some explanation: The eigenvalues,  $f$ , are normalized by the ratio of forward velocity,  $U$ , to disk radius,  $R$ . In order to obtain the frequency in Hz, the values in Table 1 must therefore be multiplied by  $U/R$ . This means that the eigenvalues are proportional to  $U$ ; as a result, all wake eigenvalues pass through the range of structural natural frequencies with increasing speed. The fundamental mode with a damped nondimensional frequency of 0.42092 is the last one to leave the vicinity of structural modes, and therefore has the most significant regarding coupling of wake and structure. Observe that for an unswept, untapered wing this nondimensional natural frequency,  $\bar{f}$ , is directly related to the traditional reduced frequency,  $k$ , like

$$k = \frac{2 \pi \bar{f}}{AR} \quad (35)$$

This means that for a wing with aspect ratio  $AR = 2\pi$  at a reduced frequency of  $k = 0.49235$  (equivalent to the undamped natural frequency of the first wake mode) the basic wake mode passes through a circle in the complex plane with the radius of the oscillation frequency. In other words, above this reduced frequency, coupling with wake modes is unavoidable. With increasing reduced frequency, the number of wake modes entering this circle increases, and thus more and more wake-structures coupling opportunities occur.

It is reassuring to note from Fig. 5 that the basic (lowest frequency) wake mode in fact resembles the induced flow field around a lifting surface in steady flow. The higher order modes are not that easy to

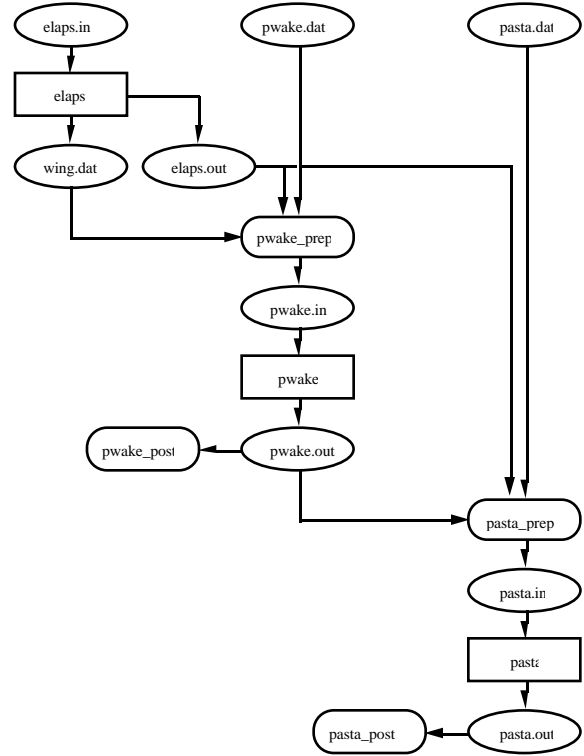


**Fig. 4: Data Flow, coupled Proprotor/  
Wing Aeroelastic Analysis**

**Table 1: Wake Eigenvalues,  $M = 7$**

Damped Frequency *R/U	Damping [% critical]
0.42092	51.87
0.29535	82.40
0.32431	91.99
0.70271	58.08
0.91961	29.21
0.65878	74.34
1.03622	40.56
0.53306	90.64
1.40369	28.44
2.34010	63.87

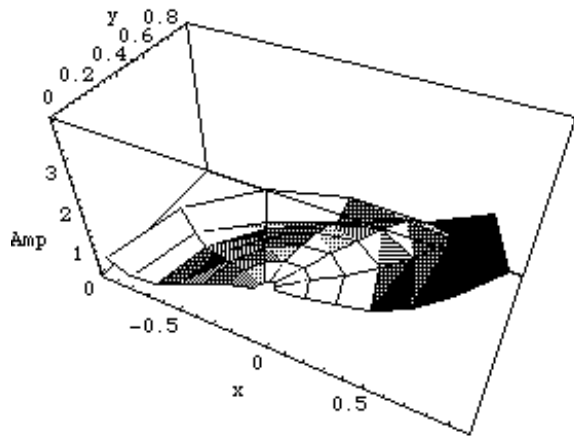


**Fig. 5: Amplitude, Wake Mode  $\bar{f} = 0.42092$**

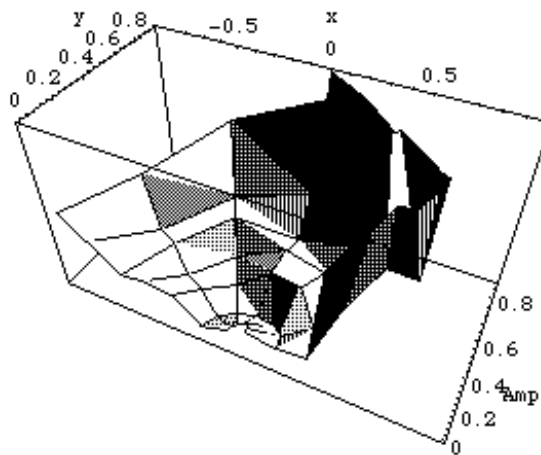


**Fig. 6: Amplitude, Wake Mode  $\bar{f} = 0.53306$**

interpret, but it seems that the highly damped eigenforms show a large increase of inflow amplitude in the vicinity of the wing tip, like in Fig. 6. One is tempted to see here the effect of a tip vortex, and the associated dissipation of energy; however, the wake model is purely inviscid and incompressible. A rigorous interpretation of this effect can not be given at this time.

As an application study, the effect of wing unsteady aerodynamics on proprotor/wing eigenvalues has been investigated. The key data of the configuration are summarized in the Appendix. Test runs have been conducted with quasi-steady

aerodynamics (in all plots the solid lines), lifting line model/numerical integration, and maximum order of radial polynomials of 7 and 15. Wing mode 1 is dominated by beamwise bending, with a positive pitch contribution (forward sweep effect); mode 2 is primarily chordwise motion, with a small negative beamwise and negative pitch contribution (nacelle pitch mode); mode 3 is the second chordwise, or nacelle yaw mode; and mode 4 is the second beamwise bending, or nacelle roll mode. Analysis of the mode shapes emphasizes the dominance of the nacelle inertias in the dynamic characteristics. The wing is only slightly modified from a design that showed stability up to a forward flight speed of about 780 ft/sec without aerodynamic damping of the wing [15]; thus, no instability was expected in the investigated velocity range.

Fig. 7 shows the frequencies as a function of velocity. Wing modes 3 and 4 are located around 23 and 48 Hz, respectively, and are therefore off the scale. Wing aerodynamics do not appear to affect the system behavior at all, since results for both wing unsteady aerodynamics and no wing aerodynamics differ only insignificantly from the quasi-steady results.

The effect of unsteady aerodynamics becomes more apparent in the damping plots, Fig. 8 - 10. Note that numerical integration and lifting line results match closely for this configuration with moderate aspect ratio and small wing sweep angle. Damping levels of the wing modes are generally low, with a maximum value around 8% for the first bending mode. This explains the very small effect on the frequencies. Fig. 8 and 9 indicate that wake feedback reduces the aerodynamic damping, particularly of the modes that are dominated by beamwise bending. The reduction in damping is more pronounced in the case of the higher resolution wake model (Fig. 9 and 10). Experience with the wake model has shown, that this must not necessarily be a sign for convergence; correlation of the results obtained using PWAKE is therefore mandatory.

Fig. 8 to 10 show negligible affect of fixed wing aerodynamics on the rotor-dominated modes. The reason for this somewhat disappointing result is seen in the fact that the chosen velocity range ends at least 100 ft/sec below the anticipated flutter speed. Serious coupling between wing and rotor modes - in other words: initiation of proprotor whirl flutter - will only be detectable in the vicinity of the flutter boundary. Hence, wing damping hardly affects the rotor modes.

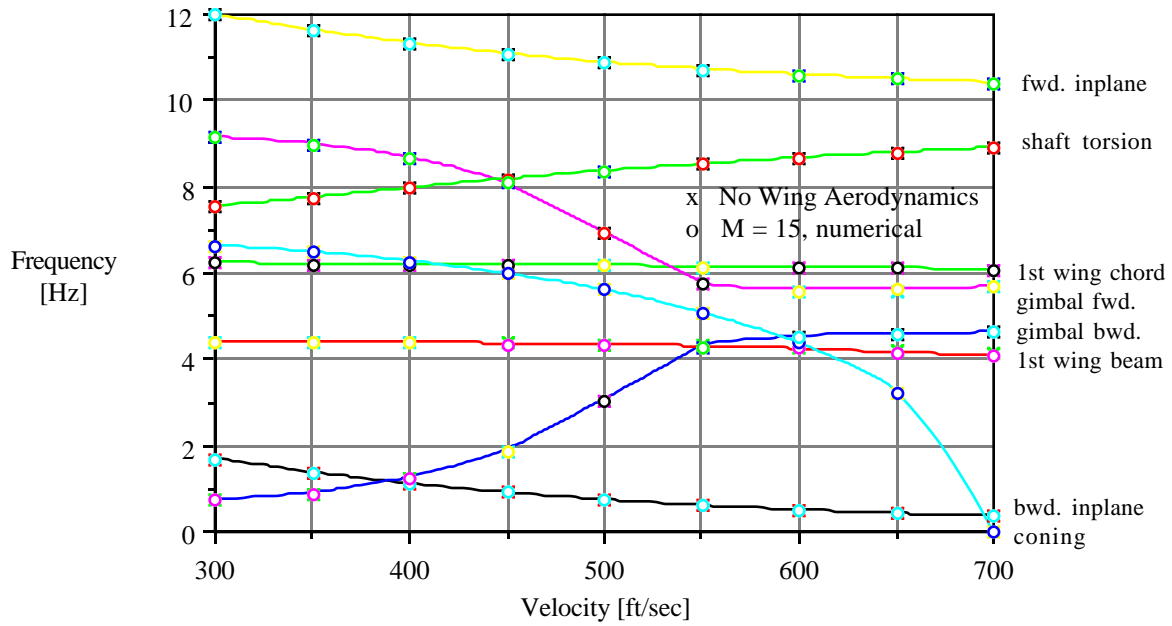


Fig. 7: Frequencies - No /Quasi-Steady / Unsteady Wing Aerodynamics

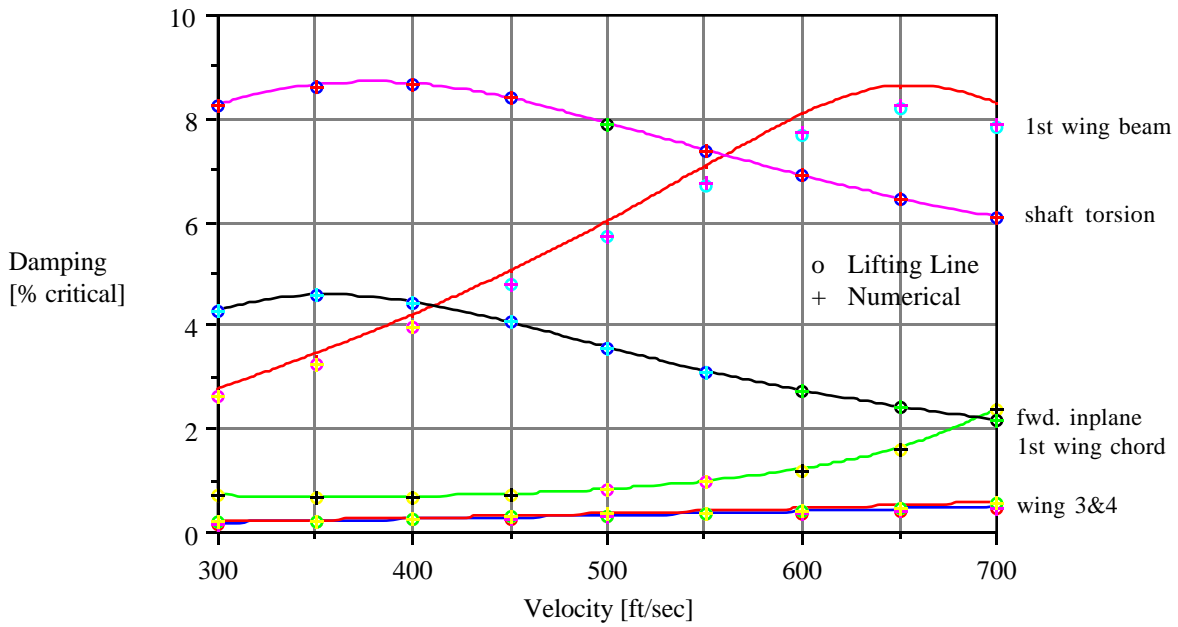


Fig. 8: Damping - Quasi-Steady and Unsteady, M = 7

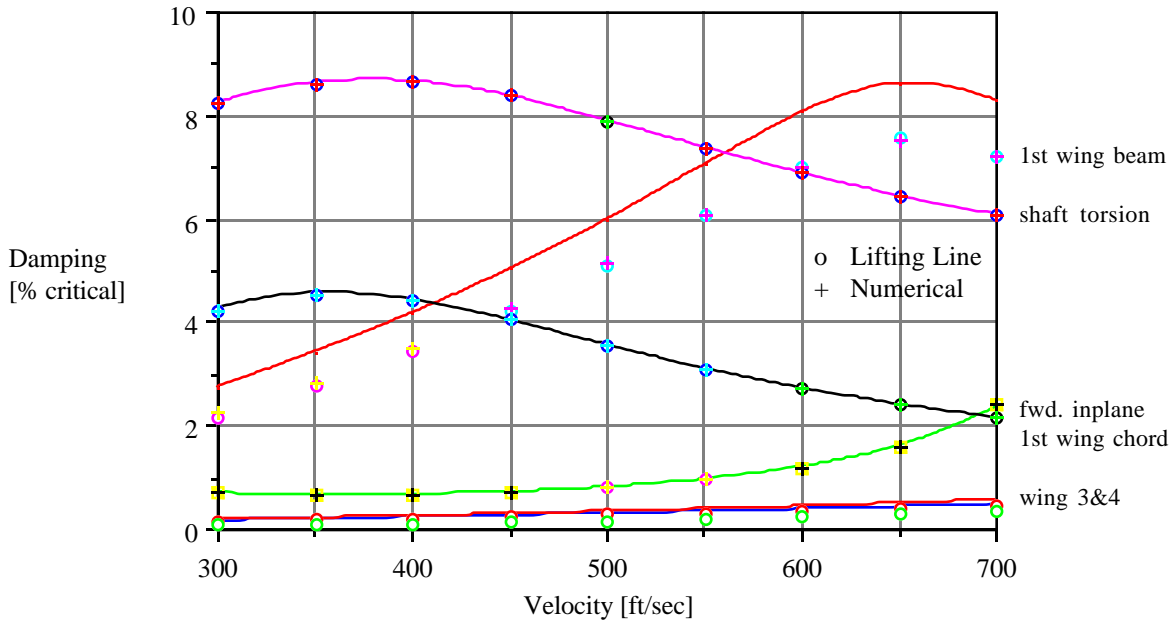


Fig. 9: Damping - Quasi-Steady and Unsteady, M = 15

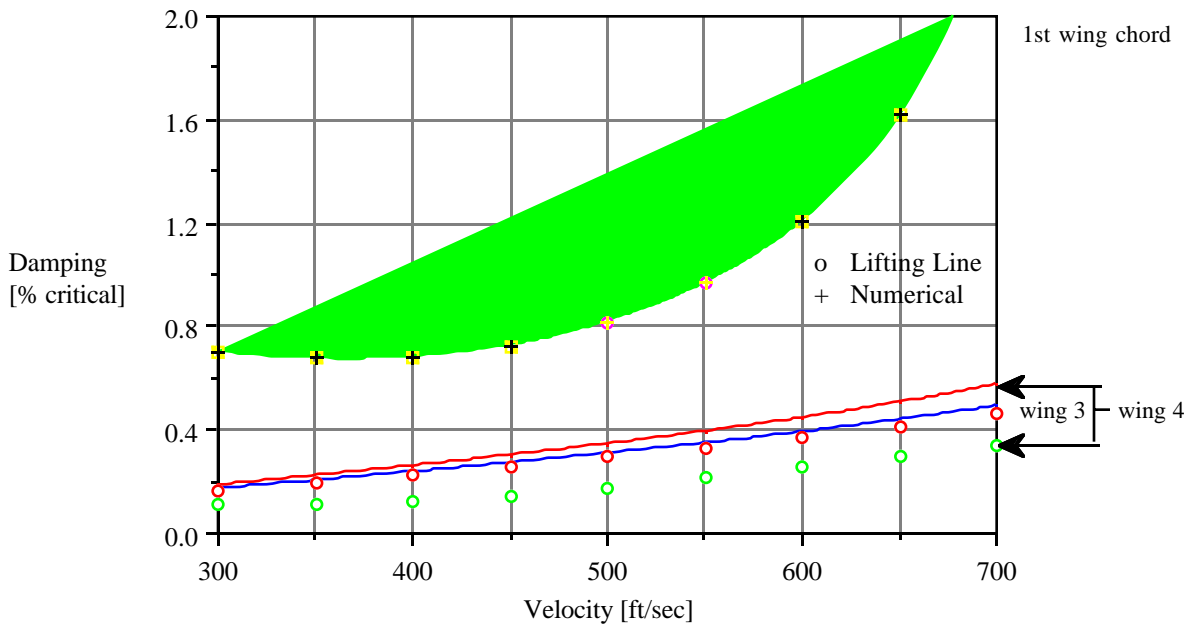


Fig. 10: Damping - Quasi-Steady and Unsteady, M = 15 (Zoom)

## Conclusions

The Peters/He wake model appears to perform well in modeling fixed-wing unsteady aerodynamics. The results show anticipated tendencies, however, correlation with established methodologies is mandatory. This is especially the case for low aspect ratio wings, where concerns regarding convergence remain.

For the investigated wing-rotor system, unsteady aerodynamic effects are detectable. Yet, due to an overall low damping level and choice of a small range of velocities below the anticipated flutter speed, the effects are not significant. A closer look at the modal behavior around the stability boundary must be taken.

### Appendix: Key Data of Proprotor/Wing Model

#### Wing

Span	50.1 ft
Aspect Ratio	6
Taper Ratio	1.0
Sweep	-5°
Thickness/Chord Ratio	0.23
Ply Thicknesses:	
0°, root	0.54 in
0°, tip (linearly tapered)	0.14 in
+45° (constant)	0.036 in
- 45° (constant)	0.015 in
Spar Cap Areas (two spars, upper spar only):	
root	0.9 in <sup>2</sup>
tip (linearly tapered)	0.57 in <sup>2</sup>

#### Rotor/Nacelle

Nacelle Weight	3720 lb
Rotor Radius	18.4 ft
Number of Blades	4
Rotor rpm	300
Natural Frequencies	
Gimbal Tilt	1.02/rev
Blade, 1 <sup>st</sup> inplane (uncoupled)	1.6/rev
Blade, 1 <sup>st</sup> out of plane (uncoupled)	1.3/rev

### Acknowledgments

Implementation of the unsteady aerodynamics program PWAKE and development of the Tiltrotor Integrated Design and Analysis Tool, tridat!, was funded by the Sikorsky Aircraft Division of the United Technologies Corporation.

## References

- [1] Schleicher, D.R., Phillips, J.D., and Carbajal, K.B., "Design Optimization of High-Speed Proprotor Aircraft," NASA-TM-103988, April 1993
- [2] Schoen, A.H., Rosenstein, H., Stanzione, K., and Wisniewski, J.S., "User's Manual for VASCOMP II, The V/STOL Aircraft Sizing and Performance Computer Program," Boeing Vertol Company Report D8-0375, Vol. VI, Third Revision, May 1980
- [3] Frick, J., and Johnson, W., "Optimal Control Theory Investigation of Proprotor/Wing Response to Vertical Gust," NASA-TM-X-62384, September 1974
- [4] Nixon, M.W., "Parametric Studies for Tiltrotor Aeroelastic Stability in High-Speed Flight," 33rd AIAA/ASME/ASCE/AHS Structures, Structural Dynamics, and Materials Conference, Dallas, Texas, April 13-15, 1992
- [5] Stettner, M., and Schrage, D.P., "An Approach to Tiltrotor Wing Aeroservoelastic Optimization through Increased Productivity," 4th AIAA/USAF/NASA/OAI Symposium on Multidisciplinary Analysis and Optimization, Cleveland, Ohio, September 21-23, 1992
- [6] Giles, G.L., "Equivalent Plate Analysis of Aircraft Wing Box Structures with General Planform Geometry," *Journal of Aircraft*, Vol. 23, No. 11, November 1986, p. 859-864
- [7] van Aken, J.M., "Alleviation of Whirl-Flutter on Tiltrotor Aircraft using Active Controls," 47th Annual Forum of the American Helicopter Society, Phoenix, Arizona, May 6-8, 1991
- [8] Liebst, B.S., Garrard, W.L., and Farm, J.A., "Design of a Multivariable Flutter Suppression / Gust Load Alleviation System," *Journal of Guidance*, Vol. 11, No. 3, May-June 1988, p. 220-229
- [9] Peters, D.A., Boyd, D.D., and He, C.J., "Finite-State Induced-Flow Model for Rotors in Hover and in Forward Flight," *Journal of the American Helicopter Society*, Vol. 34, No. 4, October 1989

- [10] Nibbelink, B.D., and Peters, D.A., "Flutter Calculations for Fixed and Rotating Wings with State-Space Inflow Dynamics," 34th AIAA / ASME / ASCE / AHS / ASC Structures, Structural Dynamics, and Materials Conference, La Jolla, California, April 19-22, 1992
- [11] Wang, Y.-R., "The Effect of Wake Dynamics on Rotor Eigenvalues in Forward Flight," Ph.D. Thesis, Georgia Institute of Technology, May 1992
- [12] Peters, D.A., and Su, A., "An Integrated Airloads-Inflow Model for Use in Rotor Aeroelasticity and Control Analysis," 47th Annual Forum of the American Helicopter Society, Phoenix, Arizona, May 6-8, 1991
- [13] Johnson, W. *Helicopter Theory*, Princeton University Press, Princeton, New Jersey, 1980, p. 477 - 478
- [14] Kvaternik, R.G., "Studies in Tiltrotor VTOL Aircraft Aeroelasticity," PhD Dissertation, Department of Solid Mechanics, Case Western Reserve, June 1973
- [15] Friehmelt, H., "Design of a Tiltrotor Wing for a EUROFAR-type Configuration," Diploma Thesis, Technische Universität Braunschweig/ Georgia Institute of Technology, March 1993